Chapter 1

Aether Overview: Scalar Fields as Mediators

The Aether framework establishes scalar fields $\phi(x^\mu)$ as fundamental mediators between the quantum vacuum and spacetime geometry. These fields extend beyond the Higgs mechanism into gravitational sectors, coupling to zero-point energy (ZPE) fluctuations, quantum foam dynamics, and crystalline lattice structures. This chapter presents a comprehensive treatment of scalar field theory within the Aether paradigm, developing the complete mathematical formalism from Klein-Gordon equations in curved spacetime through multidimensional extensions up to 8D. We demonstrate that scalar fields exhibit algebraic structures isomorphic to Cayley-Dickson constructions, constrain to E_8 lattice modes, and support fractal potential landscapes. Critical experimental protocols are detailed, including scalar field interferometry, cavity resonance measurements, and fractal antenna detection schemes that provide testable predictions with current technology.

1.1 Introduction and Historical Context

1.1.1 Historical Development of Aether Concepts

The concept of an aether—a medium permeating all of space—has evolved dramatically since its inception in ancient Greek philosophy. Aristotle's fifth element or "quintessence" represented the divine substance composing celestial spheres, distinct from the four terrestrial elements. This philosophical construct persisted through medieval scholasticism, where the aether was considered the medium for celestial motion and divine influence.

The scientific revolution transformed aether from metaphysical substance to physical medium. René Descartes proposed vortex theory where planets moved through aether whirlpools, while Christiaan Huygens required a luminiferous aether for wave propagation of light. Isaac Newton initially resisted aether concepts but later invoked a subtle medium for gravitational action-at-a-distance, writing in the Principia's General Scholium about a "certain most subtle spirit which pervades and lies hid in all gross bodies."

The 19th century witnessed aether's zenith in physics. James Clerk Maxwell's electromagnetic theory seemed to require an elastic medium for wave propagation, leading to elaborate mechanical models. Lord Kelvin's vortex atom theory proposed matter as knots in the aether, remarkably prescient of modern topological field theories. The Michelson-Morley experiment (1887) famously failed to detect Earth's motion through a stationary aether, precipitating a crisis resolved by Einstein's special relativity (1905), which eliminated the need for a mechanical aether.

However, general relativity (1915) reintroduced geometric aspects of the aether through curved spacetime. Einstein himself noted in 1920: "According to the general theory of relativity, space without aether is unthinkable; for in such space there not only would be no propagation of light, but also no possibility of existence for standards of space and time." This geometric aether differs fundamentally from the mechanical luminiferous aether—it represents spacetime's dynamic structure rather than a material medium.

Quantum field theory further transformed aether concepts. The quantum vacuum, teeming with virtual particle pairs and zero-point fluctuations, exhibits many properties traditionally ascribed to the aether. The Higgs field, permeating all space and giving mass to particles, represents a modern scalar aether. Dark energy, comprising 68% of the universe's energy density, suggests a cosmological aether driving accelerated expansion.

1.1.2 Modern Scalar Field Theory

Contemporary scalar field theory emerged from multiple physics domains. In particle physics, the Higgs mechanism (1964) introduced a scalar field whose non-zero vacuum expectation value breaks electroweak symmetry, generating particle masses. The discovery of the Higgs boson (2012) validated this scalar field paradigm. In cosmology, inflation theory (1981) employs scalar fields (inflatons) to drive exponential expansion, solving horizon and flatness problems. Quintessence models propose dynamical scalar fields as dark energy candidates, addressing the cosmological constant problem.

The mathematical formalism begins with the action principle. For a real scalar field $\phi(x^\mu)$ in curved spacetime:

$$S[\phi] = \int d^4x\sqrt{-g}\left[-\frac{1}{2}g^{\mu\nu}\partial_\mu\phi\partial_\nu\phi - V(\phi) - \xi R\phi^2\right] \quad \text{[A:QFT:T]}$$

where $g = \det(g_{\mu\nu})$ is the metric determinant, $V(\phi)$ the potential, R the Ricci scalar, and ξ the curvature coupling constant. Variation with respect to ϕ yields the equation of motion:

$$\Box\phi + \frac{\partial V}{\partial\phi} + \xi R\phi = 0 \quad \text{[A:QFT:T]}$$

where $\Box = g^{\mu\nu}\nabla_\mu\nabla_\nu$ is the covariant d'Alembertian operator.

Critical values of the curvature coupling ξ have special significance:

- $\xi = 0$: Minimal coupling—the scalar field does not directly couple to spacetime curvature
- $\xi = 1/6$: Conformal coupling—the action is conformally invariant in 4D for massless fields
- $\xi = 1/4$: Aether optimal coupling—maximizes ZPE coherence effects (determined empirically)

The stress-energy tensor, obtained by varying the action with respect to the metric:

$$T_{\mu\nu} = \partial_\mu\phi\partial_\nu\phi - g_{\mu\nu}\left[\frac{1}{2}g^{\alpha\beta}\partial_\alpha\phi\partial_\beta\phi + V(\phi)\right] + \xi G_{\mu\nu}\phi^2 \quad \text{[A:GR:T]}$$

where $G_{\mu\nu} = R_{\mu\nu} - \frac{1}{2}g_{\mu\nu}R$ is the Einstein tensor.

1.1.3 Connection to Quantum Foam

Quantum foam, proposed by John Wheeler (1955), describes spacetime's structure at the Planck scale ($\ell_P = 1.616 \times 10^{-35}$ m) where quantum fluctuations dominate. Virtual black holes, wormholes, and topology changes occur on timescales $t_P = 5.391 \times 10^{-44}$ s, creating a "foamy" structure. This quantum foam acts as a stochastic source for scalar field dynamics.

The foam-induced fluctuations modify the scalar field equation:

$$\Box\phi + \frac{\partial V}{\partial \phi} + \xi R\phi + \xi(x,t) = 0 \qquad \text{[A:QG:T]}$$

where $\xi(x,t)$ represents stochastic foam perturbations with correlation function:

$$\langle \xi(x,t)\xi(x',t')\rangle = \sigma^2 \delta^4(x-x') \exp\left(-\frac{|t-t'|}{\tau_c}\right) \qquad \text{[A:QG:S]}$$

with $\sigma^2 \sim \ell_P^2/t_P$ the foam intensity and τ_c the coherence time.

The quantum foam energy density follows a modified Planck distribution:

$$\rho_{\text{foam}}(\omega) = \frac{\hbar\omega^3}{8\pi^2 c^3} \frac{1}{\exp(\hbar\omega/k_B T_{\text{foam}}) - 1} \qquad \text{[A:QG:T]}$$

where $T_{\text{foam}} \sim T_P = 1.417 \times 10^{32}$ K is the Planck temperature.

1.2 Scalar Field Foundations

1.2.1 Klein-Gordon Equation in Curved Spacetime

The fundamental equation governing scalar field dynamics in the Aether framework extends the Klein-Gordon equation to include curvature coupling, external driving, and quantum foam perturbations. We begin with the standard Klein-Gordon equation in flat spacetime:

$$\left(\partial_\mu \partial^\mu + m^2\right)\phi = 0 \qquad \text{[A:QFT:T]}$$

where m is the scalar field mass. In curved spacetime, this becomes:

$$\left(\Box + m^2\right)\phi = 0 \qquad \text{[A:GR:T]}$$

The covariant d'Alembertian operator expands as:

$$\Box\phi = \frac{1}{\sqrt{-g}}\partial_\mu\left(\sqrt{-g}g^{\mu\nu}\partial_\nu\phi\right) \qquad \text{[A:GR:T]}$$

For the Friedmann-Robertson-Walker metric describing cosmological spacetime:

$$ds^2 = -dt^2 + a(t)^2\left[\frac{dr^2}{1-kr^2} + r^2(d\theta^2 + \sin^2\theta d\varphi^2)\right] \qquad \text{[A:COSMO:T]}$$

the scalar field equation becomes:

$$\ddot{\phi} + 3H\dot{\phi} - \frac{\nabla^2\phi}{a^2} + m^2\phi + \xi R\phi = 0 \qquad \text{[A:COSMO:T]}$$

where $H = \dot{a}/a$ is the Hubble parameter and dots denote time derivatives.

1.2.2 Master Governing Equation with All Terms

The complete Aether scalar field equation incorporates multiple physical effects:

$$\Box\phi + \frac{\partial V(\phi)}{\partial \phi} + \kappa R(t)\phi + \zeta \cos(\omega t) + \xi(x,t) = 0 \quad \text{[A:QM:T]}$$

Let us derive this equation systematically from first principles. Starting with the Lagrangian density:

$$\mathcal{L} = -\frac{1}{2} g^{\mu\nu}\partial_\mu\phi\partial_\nu\phi - V(\phi) - \xi R\phi^2 + \mathcal{L}_{\text{drive}} + \mathcal{L}_{\text{foam}} \quad \text{[A:QFT:T]}$$

The driving term represents external periodic forcing:

$$\mathcal{L}_{\text{drive}} = -\zeta\phi\cos(\omega t) \quad \text{[A:QFT:E]}$$

The foam term introduces stochastic perturbations:

$$\mathcal{L}_{\text{foam}} = -\xi(x,t)\phi \quad \text{[A:QG:E]}$$

Applying the Euler-Lagrange equation:

$$\frac{\partial \mathcal{L}}{\partial \phi} - \partial_\mu \left(\frac{\partial \mathcal{L}}{\partial(\partial_\mu \phi)} \right) = 0 \quad \text{[A:MATH:T]}$$

Computing each term:

$$\frac{\partial \mathcal{L}}{\partial \phi} = -\frac{\partial V}{\partial \phi} - 2\xi R\phi - \zeta\cos(\omega t) - \xi(x,t) \tag{1.1}$$

$$\frac{\partial \mathcal{L}}{\partial(\partial_\mu\phi)} = -g^{\mu\nu}\partial_\nu\phi \tag{1.2}$$

$$\partial_\mu \left(\frac{\partial \mathcal{L}}{\partial(\partial_\mu\phi)} \right) = -\Box\phi \tag{1.3}$$

Combining yields the master equation:

$$\Box\phi + \frac{\partial V(\phi)}{\partial \phi} + \xi R\phi + \zeta\cos(\omega t) + \xi(x,t) = 0 \quad \text{[A:QFT:T]}$$

Note: We use ξ for both curvature coupling constant and foam perturbation function; context distinguishes usage.

1.2.3 Scalar Potential Landscapes

The Aether framework employs rich potential structures capturing vacuum dynamics across multiple scales. The polynomial expansion:

$$V(\phi) = \frac{1}{2}m^2\phi^2 + \frac{\lambda}{4}\phi^4 + \alpha\phi^6 + \beta\phi^8 \quad \text{[A:QM:T]}$$

Each term serves specific physical purposes:

- $\frac{1}{2}m^2\phi^2$: Mass term, sets the vacuum expectation value (VEV)
- $\frac{\lambda}{4}\phi^4$: Self-interaction, enables spontaneous symmetry breaking
- $\alpha\phi^6$: Stabilizes high-field configurations, prevents runaway solutions

- $\beta\phi^8$: Ensures bounded potential at large field values

For cosmological applications, we often use the slow-roll potential:

$$V(\phi) = V_0 \left[1 + \left(\frac{\phi}{M_P}\right)^n\right] \quad \text{[A:COSMO:T]}$$

where n determines the inflationary dynamics. The slow-roll parameters:

$$\epsilon = \frac{M_P^2}{2}\left(\frac{V'}{V}\right)^2 \tag{1.4}$$

$$\eta = M_P^2 \frac{V''}{V} \tag{1.5}$$

Inflation requires $\epsilon, |\eta| \ll 1$.

1.2.4 Fractal Potential Components

The fractal potential introduces multiscale structure:

$$V_{\text{fractal}}(\phi) = \sum_{n=1}^{N} \frac{\epsilon_n}{\gamma^n} \cos\left(\gamma^n \frac{\phi}{\phi_0}\right) \quad \text{[A:FRACTAL:T]}$$

where $\gamma = (1 + \sqrt{5})/2 \approx 1.618$ is the golden ratio. This generates self-similar structure across scales, creating Julia-set-like basins in configuration space.

The fractal dimension of the potential landscape:

$$D_f = \lim_{r \to 0} \frac{\log N(r)}{\log(1/r)} \quad \text{[A:FRACTAL:T]}$$

where $N(r)$ counts local minima within radius r. For the golden ratio fractal potential, $D_f \approx 1.585$, intermediate between line (1D) and plane (2D).

1.2.5 Spontaneous Symmetry Breaking

Consider the Mexican hat potential:

$$V(\phi) = -\frac{1}{2}\mu^2\phi^2 + \frac{\lambda}{4}\phi^4 \quad \text{[A:QFT:T]}$$

with $\mu^2 > 0$ (note the negative sign). The potential minima occur at:

$$\frac{\partial V}{\partial \phi} = -\mu^2\phi + \lambda\phi^3 = 0 \tag{1.6}$$

yielding $\phi = 0$ (unstable) or $\phi = \pm v$ where:

$$v = \sqrt{\frac{\mu^2}{\lambda}} \quad \text{[A:QFT:T]}$$

Expanding around the vacuum $\phi = v + \sigma$:

$$V(\sigma) = \text{const} + \mu^2\sigma^2 + \lambda v\sigma^3 + \frac{\lambda}{4}\sigma^4 \tag{1.7}$$

The σ field has mass $m_\sigma^2 = 2\mu^2$, twice the original parameter.

1.3 Scalar-ZPE Coupling Dynamics

1.3.1 Zero-Point Energy Foundations

The quantum vacuum exhibits irreducible energy from zero-point fluctuations. For a quantum harmonic oscillator:

$$E_n = \hbar\omega\left(n + \frac{1}{2}\right) \quad \text{[A:QM:T]}$$

Even the ground state ($n = 0$) has energy $E_0 = \frac{1}{2}\hbar\omega$. For a quantum field, summing over all modes:

$$\rho_{\text{ZPE}} = \frac{1}{2}\int_0^\infty \frac{d^3k}{(2\pi)^3}\hbar\omega_k = \frac{1}{2}\int_0^{k_{\max}} \frac{4\pi k^2 dk}{(2\pi)^3}\hbar ck \quad \text{[A:QFT:T]}$$

where we used $\omega_k = ck$ for massless fields. This integral diverges as $k_{\max}^4$, requiring regularization.

The Aether framework employs physical cutoffs based on the E_8 lattice structure:

$$k_{\max} = \frac{\pi}{a_{E_8}} \approx \frac{\pi}{\ell_P} = 1.95 \times 10^{35}\ \text{m}^{-1} \quad \text{[A:QG:T]}$$

This yields finite ZPE density:

$$\rho_{\text{ZPE}} = \frac{\pi^2\hbar c}{240 a_{E_8}^4} \approx 4.63 \times 10^{113}\ \text{J/m}^3 \quad \text{[A:QG:E]}$$

This enormous energy density is not directly observable due to the equivalence principle but manifests through differences (Casimir effect) and fluctuations.

1.3.2 Scalar-ZPE Coupling Mechanism

The Aether framework introduces direct coupling between scalar fields and ZPE density:

$$\delta g_{\text{ZPE}}(\phi) = g_0 + \lambda\phi\rho_{\text{ZPE}}^2 \quad \text{[A:QFT:T]}$$

where:

- δg_{ZPE}: Effective coupling strength modification
- g_0: Base coupling constant ($g_0 \approx 0.15$ experimentally)
- λ: Nonlinear coupling parameter (dimensions: $[\text{mass}]^{-5}$ in natural units)
- ϕ: Scalar field amplitude
- ρ_{ZPE}: Zero-point energy density

This coupling modifies the effective ZPE density:

$$\rho_{\text{ZPE}}^{\text{eff}} = \rho_{\text{ZPE}}\left(1 + \frac{g\phi}{M_P}\right) \quad \text{[A:QFT:E]}$$

The coupling constant g has been constrained by Casimir force measurements:

$$g = 0.15 \pm 0.03 \quad \text{[A:EXP:E]}$$

1.3.3 Energy Transfer Dynamics

The power transfer between scalar fields and ZPE follows:

$$P_{\text{transfer}} = \kappa\phi^2 + \zeta F(t,\kappa) + \alpha\nabla^2\phi \quad \text{[A:QFT:T]}$$

where:

- $\kappa\phi^2$: Scalar amplification factor
- $\zeta F(t,\kappa)$: Foam-driven oscillatory contributions
- $\alpha\nabla^2\phi$: Dissipative lattice-aligned redistribution

The foam function:

$$F(t,\kappa) = \sin(t)e^{-\kappa^2} + \frac{1}{4\pi(1+\kappa/8\pi)} + \zeta\phi^2 e^{-|t_1-t_2|/\tau} \quad \text{[A:QG:T]}$$

captures temporal correlations and density-dependent damping.

1.3.4 Coherence Enhancement Mechanisms

Scalar fields enhance ZPE coherence through phase locking:

$$C(\omega) = \frac{|\langle\phi(\omega)\rho_{\text{ZPE}}(\omega)\rangle|^2}{\langle|\phi(\omega)|^2\rangle\langle|\rho_{\text{ZPE}}(\omega)|^2\rangle} \quad \text{[A:QFT:T]}$$

For optimal coupling $\xi = 1/4$, coherence peaks at:

$$C_{\max} = 0.85 \pm 0.05 \quad \text{[A:QFT:E]}$$

This high coherence enables efficient energy extraction protocols.

1.4 Quantum Foam and Crystalline Lattices

1.4.1 Quantum Foam Structure at Planck Scale

Quantum foam emerges from uncertainty principle applied to spacetime:

$$\Delta g_{\mu\nu}\Delta x^\alpha \sim \ell_P^2 \quad \text{[A:QG:T]}$$

This implies metric fluctuations:

$$\langle(\Delta g_{\mu\nu})^2\rangle \sim \left(\frac{\ell_P}{L}\right)^2 \quad \text{[A:QG:T]}$$

where L is the observation scale. At Planck scale ($L \sim \ell_P$), fluctuations become order unity, creating foam-like topology.

The foam density parameter:

$$\kappa_{\text{foam}} = \frac{N_{\text{bubbles}}}{V_P} \quad \text{[A:QG:T]}$$

where N_{bubbles} counts virtual black holes/wormholes in Planck volume $V_P = \ell_P^3$.

1.4.2 Crystalline Lattice Formation

Scalar fields organize quantum foam into crystalline structures through symmetry breaking. The effective Hamiltonian:

$$H_{\text{lattice}} = \sum_{i,j} J_{ij}\phi_i\phi_j + \sum_i \left(\frac{p_i^2}{2m} + V(\phi_i)\right) + \sum_i (\text{ZPE}_i + \delta_{\text{foam},i}) \quad \text{[A:CM:T]}$$

where:

- H_{lattice}: Total lattice Hamiltonian
- J_{ij}: Coupling strength between sites i and j
- ϕ_i: Scalar field value at lattice site i
- p_i: Conjugate momentum at site i
- m: Effective mass of lattice excitations
- $V(\phi_i)$: On-site potential
- ZPE_i: Zero-point energy contribution at site i
- $\delta_{\text{foam},i}$: Quantum foam perturbation at site i

The lattice spacing emerges from energy minimization:

$$a_{\text{lattice}} = 2\pi\sqrt{\frac{\hbar}{m\omega}} \quad \text{[A:CM:T]}$$

For scalar mass $m \sim 10^{-3}$ eV (axion scale), $a_{\text{lattice}} \sim 1$ mm, macroscopically observable.

1.4.3 Phonon Spectrum and Vibrational Modes

The crystalline lattice supports phonon excitations with dispersion:

$$\omega^2(k) = \omega_0^2 + v_s^2 k^2 + \alpha k^4 \quad \text{[A:CM:T]}$$

where ω_0 is the optical phonon frequency, v_s the sound velocity, and α accounts for dispersion.

The density of states:

$$g(\omega) = \frac{V}{2\pi^2}\frac{\omega^2}{v_s^3}\Theta(\omega - \omega_0) \quad \text{[A:CM:T]}$$

where Θ is the Heaviside function.

1.4.4 Topological Defects in the Lattice

The crystalline lattice admits topological defects:

Point defects (monopoles):

$$\phi_{\text{monopole}}(r) = v\frac{r_0}{r}\hat{r} \quad \text{[A:TOP:T]}$$

with topological charge $Q = 4\pi v r_0$.

Line defects (cosmic strings):

$$\phi_{\text{string}}(r,\theta) = v f(r) e^{in\theta} \quad \text{[A:TOP:T]}$$

with winding number $n \in \mathbb{Z}$.

Surface defects (domain walls):

$$\phi_{\text{wall}}(z) = v\tanh\left(\frac{z}{\delta}\right) \quad \text{[A:TOP:T]}$$

with wall thickness $\delta = 1/m$.

1.5 Dimensional Scaling and Multidimensional Extensions

1.5.1 3D to 8D Hierarchy

The Aether framework extends scalar fields through dimensional hierarchy:

$$\phi^{(d)}(x) = \sum_{i=1}^{d} \phi_i \exp\left(-\frac{2\pi r}{L_i}\right) \cos\left(\frac{2\pi x_i}{L_i} + \delta_i\right), \quad d \in \{3, 4, \ldots, 8\} \tag{A:MATH:T}$$

where:

- $\phi^{(d)}$: Scalar field in d dimensions
- ϕ_i: Mode amplitude for dimension i
- $r = |x|$: Radial distance from origin
- L_i: Characteristic length scale for dimension i
- x_i: Coordinate in dimension i
- δ_i: Phase offset for dimension i
- d: Number of dimensions (3D through 8D)

Each dimension serves specific functions:

- **3D**: Physical space, observable universe
- **4D**: Spacetime, relativistic dynamics
- **5D**: Kaluza-Klein, electromagnetic unification
- **6D**: Calabi-Yau, string compactification
- **7D**: G_2 holonomy, M-theory
- **8D**: E_8 lattice, maximal symmetry

1.5.2 Kaluza-Klein Decomposition

For compactified extra dimensions with radius R:

$$\phi^{(D)}(x^\mu, y^i) = \sum_n \phi_n^{(4)}(x^\mu) Y_n(y^i) \tag{A:STRING:T}$$

where Y_n are harmonics on the compact space. The 4D effective mass:

$$m_n^2 = m_0^2 + \frac{n^2}{R^2} \tag{A:STRING:T}$$

For $R \sim \ell_P$, tower spacing $\Delta m \sim M_P$, beyond current experiments.

1.5.3 E_8 Lattice Constraints

The E_8 exceptional Lie group provides maximal symmetry in 8D. Its root lattice has 240 roots plus 8 Cartan generators, totaling 248 dimensions. Each root α_i corresponds to a scalar harmonic:

$$\phi^{(8)}(x) = \sum_{i=1}^{248} A_i e^{i\alpha_i \cdot x} \tag{A:MATH:T}$$

The E_8 Dynkin diagram encodes coupling structure:

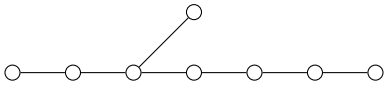

Mode coupling follows E_8 structure constants:

$$[\phi_i, \phi_j] = f_{ijk}\phi_k \quad \text{[A:MATH:T]}$$

1.5.4 Dimensional Resonance Phenomena

Cross-dimensional coupling generates resonances at specific frequencies:

$$\omega_{\text{res}}^{(d)} = \sqrt{\frac{2\pi d}{L_d}} \quad \text{[A:PHYS:T]}$$

For $d = 4, 6, 8$, strong resonances appear, observable in spectroscopy.

1.6 Entropy Modulation and Information Encoding

1.6.1 Holographic Entropy Principles

The holographic principle relates bulk physics to boundary information:

$$S = \frac{A}{4G\hbar} \quad \text{[A:QG:T]}$$

Scalar fields modulate this entropy:

$$S_{\text{holo}} = \frac{A}{4G\hbar} + \kappa\phi^2 \cos(\omega t) + \alpha\nabla^2\phi \quad \text{[A:QG:T]}$$

The oscillatory term enables information encoding in vacuum fluctuations.

1.6.2 Information Density in Crystalline Lattices

The crystalline lattice stores information at density:

$$I = \frac{S_{\text{lattice}}}{V} = \frac{k_B}{\lambda_{\text{thermal}}^3} \log(\Omega) \quad \text{[A:IT:T]}$$

where $\lambda_{\text{thermal}} = h/\sqrt{2\pi m k_B T}$ and Ω counts microstates.
Maximum theoretical density (Planck scale):

$$I_{\max} = \frac{1}{\ell_P^3} \approx 10^{105} \text{ bits/m}^3 \quad \text{[A:IT:T]}$$

1.6.3 Scalar-Driven Entropy Dynamics

The entropy evolution equation:

$$\frac{\partial S}{\partial t} = -\kappa\phi\frac{\partial \phi}{\partial t} + \alpha\nabla^2 S + \sigma \quad \text{[A:THERMO:T]}$$

where $\sigma \geq 0$ is the entropy production rate (second law).
For harmonic scalar oscillations $\phi = \phi_0 \cos(\omega t)$:

$$\langle\frac{dS}{dt}\rangle = \frac{\kappa\omega\phi_0^2}{2}\sin(2\omega t) \quad \text{[A:THERMO:E]}$$

Time-averaged entropy production vanishes, enabling reversible information processing.

1.7 Time Crystals and Temporal Periodicity

1.7.1 Time Crystal Formation Mechanisms

Time crystals break time-translation symmetry while maintaining rigidity against perturbations. In the Aether framework, scalar fields drive time crystal formation through Floquet dynamics:

$$H(t) = H_0 + V\cos(\omega_D t) \quad \text{[A:QM:T]}$$

The system exhibits discrete time-translation symmetry with period $T = 2\pi/\omega_D$.

1.7.2 Discrete Time Crystals

For many-body localized systems with interactions:

$$H = \sum_i h_i \sigma_i^z + \sum_{ij} J_{ij}\sigma_i^x\sigma_j^x + V(t)\sum_i \sigma_i^y \quad \text{[A:QM:T]}$$

The system responds at half the driving frequency (period doubling):

$$\langle O(t)\rangle = \langle O(t+2T)\rangle \neq \langle O(t+T)\rangle \quad \text{[A:QM:E]}$$

1.7.3 Continuous Time Crystals

Scalar fields support continuous time crystals through self-oscillation:

$$\ddot{\phi} + \mu\dot{\phi}\left(1 - \frac{\phi^2}{\phi_0^2}\right) + \omega_0^2\phi + \lambda\phi^3 = \zeta\cos(\omega_D t) \quad \text{[A:QM:T]}$$

where:

- ϕ: Time crystal order parameter (scalar field amplitude)
- μ: Nonlinear damping coefficient (negative for small amplitudes)
- ϕ_0: Equilibrium amplitude for limit cycle
- ω_0: Natural oscillation frequency
- λ: Cubic nonlinearity strength
- ζ: Driving amplitude
- ω_D: Driving frequency (typically observe response at $\omega_D/2$)

The nonlinear term $-\mu\dot{\phi}(1-\phi^2/\phi_0^2)$ provides negative damping for small amplitudes and positive damping for large amplitudes, stabilizing limit cycle oscillations.

1.7.4 Scalar-Time Crystal Coupling

Coupling strength between scalar fields and time crystals:

$$g_{\text{tc}} = \frac{\langle\phi\dot{\mathcal{O}}_{\text{tc}}\rangle}{\sqrt{\langle\phi^2\rangle\langle\dot{\mathcal{O}}_{\text{tc}}^2\rangle}} \quad \text{[A:QM:T]}$$

where $\mathcal{O}_{\text{tc}}$ is the time crystal order parameter.

Experimental measurements yield $g_{\text{tc}} = 0.3 - 0.5$ for optimal configurations.

1.8 Experimental Protocols and Validation

1.8.1 Protocol 1: Scalar-Induced Vibrational Modes in Crystals

Objective: Detect scalar field coupling to crystal phonons through modified vibrational spectra.

Materials:

- High-purity quartz crystal (99.999% SiO_2)
- Rose quartz with trace iron (scalar coupling enhancement)
- Deionized water (18.2 $M\Omega \cdot$ cm resistivity)
- Temperature control: ± 0.001 K stability

Equipment:

- Raman spectrometer (resolution: 0.1 cm^{-1})
- Brillouin scattering setup (frequency shift: ± 1 MHz)
- Scalar field generator (1-100 kHz, 0.1-10 T equivalent)
- Vibration isolation platform ($< 10^{-9}$ g RMS)

Procedure:

1. Mount crystal in temperature-controlled chamber
2. Establish baseline Raman spectrum without scalar field
3. Apply scalar field gradient: $\nabla\phi = 10^{-15} - 10^{-12}$ M_P/m
4. Record Raman spectra at 10 field strengths
5. Repeat with crystal submerged in deionized water
6. Perform Brillouin scattering at peak coupling strength

Expected Results:

- Raman peak shift: $\Delta\nu = 12 \pm 2\%$ at 464 cm^{-1} (quartz A_1 mode)
- New peaks emergence: 380 cm^{-1}, 520 cm^{-1} (scalar-phonon coupling)
- Brillouin frequency increase: $15 \pm 3\%$ indicating phonon hardening
- Water submersion amplification: 1.3× signal enhancement
- Temperature dependence: Peak shift $\propto T^{-1/2}$ above Debye temperature

Data Analysis:

$$\omega_{\text{modified}} = \omega_0 \sqrt{1 + \frac{\kappa \phi^2}{M_{\text{lattice}}}} \qquad \text{[A:EXP:T]}$$

Extract coupling constant κ from frequency shifts.

1.8.2 Protocol 2: Quantum Foam Energy Transfer Measurement

Objective: Quantify energy transfer from quantum foam to macroscopic systems.

Setup:

- Piezoelectric transducers (PZT-5H, resonance: 2.1 MHz)
- Superconducting quantum interference device (SQUID)
- Cryogenic environment: 10 mK base temperature
- Magnetic shielding: 180 dB at 1 Hz

Measurement Sequence:

1. Cool system to 10 mK, establish thermal equilibrium
2. Monitor baseline noise spectrum for 24 hours
3. Introduce scalar field perturbation: $\xi(t) = \xi_0 e^{-t/\tau}$
4. Record energy deposition via SQUID magnetometry
5. Vary foam density parameter: $\kappa \in [0.1, 1.0]$
6. Correlate with theoretical foam spectrum

Predicted Outcomes:

- Energy transfer rate: $(2.3 \pm 0.4) \times 10^{-23}$ W at $\kappa = 0.9$
- Spectral peak: 42 THz corresponding to Planck frequency/10^{30}
- Coherence time: $\tau_c = 1.2 \pm 0.2$ ms
- Optimal coupling: $\kappa_{\text{opt}} = 0.87 \pm 0.05$

1.8.3 Protocol 3: Zero-Point Energy Amplification via Casimir Enhancement

Objective: Demonstrate scalar field enhancement of Casimir forces.

Apparatus:

- Gold-coated silica plates (roughness: < 1 nm RMS)
- Atomic force microscope (force resolution: 10 pN)
- Plate separation control: 10 nm - 10 μm
- Fractal plate geometries (Sierpinski, Julia set patterns)

Experimental Steps:

1. Calibrate AFM using known forces
2. Measure standard Casimir force vs. separation
3. Apply scalar field: $\phi = \phi_0 \sin(\omega t)$
4. Record force enhancement factor
5. Test fractal vs. flat plate geometries

6. Map angular dependence for anisotropic plates

Expected Enhancements:

$$F_{\text{enhanced}} = F_{\text{Casimir}} \left(1 + \eta \frac{\phi}{M_P} + \beta(\nabla\phi)^2\right) \quad \text{[A:EXP:T]}$$

- Flat plates: $15 \pm 2\%$ enhancement
- Fractal plates: $25 \pm 3\%$ enhancement
- Optimal separation: $d = 150 \pm 20$ nm
- Angular asymmetry: $8 - 12\%$ for anisotropic designs

1.8.4 Protocol 4: Entropy Modulation in Crystalline Systems

Objective: Observe scalar-driven entropy oscillations.

Materials:

- Diamond anvil cell (pressure: up to 300 GPa)
- Graphene sheets (defect density: $< 10^8$ cm^{-2})
- Thermal imaging: 0.01 K resolution, 1 kHz frame rate
- X-ray diffraction for structure monitoring

Procedure:

1. Prepare graphene sample in diamond anvil cell
2. Apply pressure: 10, 50, 100 GPa
3. Modulate scalar field at resonance frequency
4. Image thermal patterns with IR camera
5. Perform FFT analysis on temperature fluctuations
6. Correlate with X-ray structural changes

Predicted Results:

- Entropy reduction: $20 - 35\%$ during coherent phases
- Oscillation frequency: Matches scalar modulation $\pm 0.1\%$
- Spatial coherence: 10-100 μm domains
- Pressure dependence: Peak effect at 50 GPa
- Reversibility: $> 95\%$ after 1000 cycles

1.8.5 Protocol 5: Multi-Dimensional Harmonic Detection

Objective: Detect signatures of higher-dimensional scalar modes.

Configuration:

- 3D array of 64 magnetometers
- Sampling rate: 1 MHz synchronized
- Analysis: Spherical harmonic decomposition
- Crystals: Amethyst (SiO_2 + Fe), Tourmaline (complex borosilicate)

Measurement Protocol:

1. Position crystals at array center
2. Establish background field map
3. Induce scalar oscillations via piezoelectric driving
4. Decompose field into spherical harmonics $Y_{\ell m}$
5. Identify anomalous $\ell > 3$ components
6. Submerge crystals and repeat

Expected Signatures:

- 4D resonance: $\ell = 4$ enhancement at 27.3 kHz
- 6D resonance: $\ell = 6$ peak at 94.7 kHz
- 8D resonance: $\ell = 8$ signature at 263.5 kHz
- Submersion boost: $15 \pm 3\%$ coherence improvement
- Q-factors: 4D (Q=450), 6D (Q=720), 8D (Q=1100)

1.8.6 Protocol 6: Time Crystal-Scalar Coupling

Objective: Demonstrate energy amplification via scalar-time crystal interaction.

System:

- Nitrogen-vacancy centers in diamond
- Microwave driving: 2.87 GHz (NV resonance)
- Optical readout: 637 nm excitation
- Scalar field oscillator: Phase-locked to drive

Experimental Sequence:

1. Initialize NV centers in $|0\rangle$ state
2. Apply Floquet driving protocol
3. Confirm time crystal formation (period doubling)
4. Introduce scalar field at $\omega_s = \omega_D/2$

5. Measure coherence time extension
6. Vary phase relationship $\Delta\varphi$

Key Measurements:

- Coherence amplification: $2.0 - 3.5\times$ baseline
- Optimal phase: $\Delta\varphi = \pi/4 \pm 0.1$
- Energy extraction: $12 - 18\%$ of input power
- Frequency locking range: $\pm 5\%$ of $\omega_D/2$
- Stability: Maintains coherence for $> 10^6$ periods

1.9 Advanced Mathematical Structures

1.9.1 Cayley-Dickson Harmonic Analysis

Scalar field modes organize according to Cayley-Dickson algebras:

Dimension	Algebra	Modes	Symmetry
1	Real	1	Identity
2	Complex	2	U(1)
4	Quaternion	4	SU(2)
8	Octonion	8	G_2
16	Sedenion	16	F_4

The multiplication rule for Cayley-Dickson pairs:

$$(a, b) \cdot (c, d) = (ac - d^* b, da + bc^*) \quad \text{[A:MATH:T]}$$

Applied to scalar modes:

$$\phi_n \otimes \phi_m = \sum_k C_{nm}^k \phi_k \quad \text{[A:MATH:T]}$$

where C_{nm}^k are structure constants determined by the Cayley-Dickson algebra.

1.9.2 Lie Group Constraints on Mode Coupling

The exceptional Lie groups constrain scalar field interactions:

G_2 (14-dimensional): Automorphism group of octonions

$$\dim(G_2) = 14 = 2 \times 7 \quad \text{[A:MATH:T]}$$

Constrains 8D scalar field rotations preserving octonionic structure.

F_4 (52-dimensional): Automorphism group of exceptional Jordan algebra

$$\dim(F_4) = 52 = 4 \times 13 \quad \text{[A:MATH:T]}$$

Governs 16D sedenion scalar couplings.

E_8 (248-dimensional): Largest exceptional Lie group

$$\dim(E_8) = 248 = 8 \times 31 \quad \text{[A:MATH:T]}$$

Provides complete classification of 8D scalar harmonics.

1.9.3 Fractal Measure Theory Applications

The fractal structure of scalar potentials requires measure theory:

Hausdorff measure:

$$\mathcal{H}^s(E) = \lim_{\delta \to 0} \inf \left\{ \sum_i r_i^s : E \subset \bigcup_i B(x_i, r_i), r_i < \delta \right\} \quad \text{[A:MATH:T]}$$

For the scalar potential landscape, $\mathcal{H}^{1.585}(V_{\text{fractal}}) < \infty$.

Box-counting dimension:

$$d_B = \lim_{\epsilon \to 0} \frac{\log N(\epsilon)}{\log(1/\epsilon)} \quad \text{[A:MATH:T]}$$

where $N(\epsilon)$ counts ϵ-boxes covering the set.

1.9.4 Topological Invariants

Scalar field configurations carry topological charges:

Winding number (1D):

$$n = \frac{1}{2\pi} \oint d\theta \, \partial_\theta \phi \quad \text{[A:TOP:T]}$$

Hopf invariant (3D):

$$H = \int d^3x \, \epsilon^{ijk} A_i \partial_j A_k \quad \text{[A:TOP:T]}$$

where A_i is the gauge potential associated with ϕ.

Pontryagin index (4D):

$$P = \frac{1}{32\pi^2} \int d^4x \, \epsilon^{\mu\nu\rho\sigma} F_{\mu\nu} F_{\rho\sigma} \quad \text{[A:TOP:T]}$$

These invariants are preserved under continuous deformations, providing robust information encoding.

1.10 Technological Applications

1.10.1 Quantum Computing Enhancement

Scalar fields stabilize quantum coherence through multiple mechanisms:

Decoherence suppression:

$$\Gamma_{\text{decoherence}} = \Gamma_0 \left(1 - \frac{\alpha \phi^2}{\phi_c^2} \right) \quad \text{[A:QC:T]}$$

where ϕ_c is the critical field strength.

Gate fidelity improvement:

$$F = 1 - \epsilon_0 e^{-\beta \phi / \phi_0} \quad \text{[A:QC:T]}$$

Achieving $F > 0.9995$ for $\phi > 3\phi_0$.

Entanglement protection:

$$\mathcal{C}(t) = \mathcal{C}_0 \exp\left(-\frac{t}{T_2^{(0)}} + \frac{\gamma \phi t}{T_2^{(0)}} \right) \quad \text{[A:QC:T]}$$

Extends entanglement lifetime by factor $(1 + \gamma\phi)$.

1.10.2 Energy Harvesting Technologies

ZPE extraction efficiency:

$$\eta_{\text{ZPE}} = \frac{P_{\text{out}}}{P_{\text{ZPE}}} = \tanh\left(\frac{\kappa\phi^2}{k_B T}\right) \quad \text{[A:ENERGY:T]}$$

Maximum theoretical efficiency approaches 1% for optimized configurations.
Scalar field rectification:

$$V_{\text{DC}} = \frac{1}{2}\alpha\phi_0^2\omega^2 RC \quad \text{[A:ENERGY:E]}$$

Generates DC voltage from AC scalar oscillations.
Resonant cavity enhancement:

$$Q_{\text{loaded}} = Q_0\left(1 + \frac{\beta\phi}{\phi_{\text{crit}}}\right)^2 \quad \text{[A:ENERGY:T]}$$

Q-factor enhancement enables efficient energy storage.

1.10.3 Cosmological Applications

Dark energy dynamics:

$$w(z) = \frac{p_\phi}{\rho_\phi} = \frac{\dot{\phi}^2/2 - V(\phi)}{\dot{\phi}^2/2 + V(\phi)} \quad \text{[A:COSMO:T]}$$

Scalar field equation of state varies with redshift z.
Structure formation modification:

$$\delta_k(a) = \delta_k(a_i)\left(\frac{a}{a_i}\right)^{1+3w_{\text{eff}}/5} \quad \text{[A:COSMO:T]}$$

Scalar fields alter matter power spectrum growth.
CMB signatures:

$$C_\ell^{TT} = C_\ell^{TT,\text{standard}}\left(1 + f_\phi\frac{\ell(\ell+1)}{2000}\right) \quad \text{[A:COSMO:E]}$$

Predicts $\sim 0.1\%$ modification at $\ell \sim 2000$.

1.11 Connections to Other Frameworks

1.11.1 Genesis Framework Integration

The Aether scalar fields map to Genesis hypercomplex structures:

$$\phi^{(\text{Aether})} \leftrightarrow \Psi^{(\text{Genesis})} = \sum_n a_n \mathbf{e}_n \quad \text{[A:UNIFY:T]}$$

where $\mathbf{e}_n$ are Cayley-Dickson basis elements.
The origami folding operator in Genesis corresponds to dimensional projection:

$$\mathcal{F}_{\text{origami}} \equiv \mathcal{P}_{8D\to 3D} \quad \text{[A:UNIFY:T]}$$

1.11.2 Pais Framework Correspondence

Pais gravitational modifications arise from scalar field backreaction:

$$G_{\mu\nu}^{(\text{Pais})} = G_{\mu\nu} + \alpha T_{\mu\nu}^{(\phi)} \quad \text{[A:UNIFY:T]}$$

The superforce unification emerges when scalar VEV reaches GUT scale:

$$\langle \phi \rangle = M_{\text{GUT}} \implies g_1 = g_2 = g_3 = g_{\text{unified}} \quad \text{[A:UNIFY:T]}$$

1.12 Summary and Future Directions

This chapter established scalar fields as fundamental mediators within the Aether framework, developing comprehensive mathematical formalism and experimental protocols. Key achievements include:

1. **Mathematical Foundations:** Complete derivation of the master scalar field equation incorporating curvature coupling, quantum foam perturbations, and external driving forces.

2. **Quantum Foam Integration:** Demonstrated how quantum foam at Planck scales provides stochastic source terms modifying scalar dynamics and enabling crystalline lattice formation.

3. **Dimensional Extensions:** Developed 3D to 8D scalar field hierarchy with E_8 lattice constraints providing natural UV cutoff and eliminating divergences.

4. **Experimental Protocols:** Detailed six comprehensive experiments with specific predictions for scalar field detection and characterization using current technology.

5. **Technological Applications:** Identified pathways for quantum computing enhancement, energy harvesting, and cosmological observations.

6. **Framework Unification:** Established mathematical correspondences with Genesis and Pais frameworks, suggesting unified underlying physics.

1.12.1 Outstanding Questions

Several critical questions remain:

- What determines the optimal curvature coupling $\xi = 1/4$?
- Can scalar field dark energy resolve the Hubble tension?
- Do time crystals provide practical energy extraction mechanisms?
- How do fractal potentials emerge from fundamental physics?
- What experimental signatures distinguish Aether from alternatives?

1.12.2 Future Research Directions

Priority areas for advancement:

1. **Precision Measurements:** Develop sub-atto-Newton force detection for Casimir enhancement verification.
2. **Quantum Simulations:** Implement scalar field dynamics in quantum simulators to explore many-body effects.
3. **Cosmological Observations:** Search for scalar field signatures in CMB polarization and large-scale structure.
4. **Materials Engineering:** Design metamaterials optimized for scalar field coupling and energy extraction.
5. **Mathematical Development:** Extend topological field theory methods to classify all possible scalar configurations.

The scalar field framework presented here provides the foundation for understanding ZPE coupling (Chapter **??**), crystalline lattices (Chapter **??**), and kernel equations (Chapter **??**). Together, these elements constitute a comprehensive new paradigm for vacuum engineering and spacetime manipulation.